

Review of microscale dynamics of dilution-induced asphaltene precipitation under controlled mixing conditions

Jia Meng, Somasekhara Goud Sontti, Xuehua Zhang*

Department of Chemical and Materials Engineering, University of Alberta, Alberta T6G 1H9, Canada

Abstract

As the most complex and heaviest component in bitumen, asphaltene precipitation induced by solvent dilution is important in oil sands extraction to remove solids and water from bitumen froth through dilution by paraffinic solvents. This review will compare asphaltene precipitation to dilution-induced solvent shifting in aqueous systems via the ouzo effect. We attempt to highlight similarities and differences in the evolution of nanodroplets and effects from solvent mixing conditions and point out mutual experimental techniques and modeling approaches for the research of both asphaltene precipitation and nanodroplet formation. The review will start from basic concepts in both asphaltene precipitation and the ouzo effect, then move on to the effects of solvent mixing on asphaltene precipitation in bulk. After that, we will introduce advances in microfluidic systems combined with cutting-edge experimental and simulation tools for asphaltene precipitation induced under controlled mixing with solvents and a droplet formation. Such comparison will inspire more in-depth understanding and control of asphaltene precipitation and the ouzo effect in aqueous systems.

Email address: xuehua.zhang@ualberta.ca (Xuehua Zhang*)

1. Introduction

Asphaltene is the most complex and heaviest component in bitumen, consisting of polycyclic aromatic species with different molecular weights, polarity, and heteroatom content. Asphaltene is insoluble in paraffinic solvents and soluble in aromatic solvents [1]. Asphaltene precipitation is triggered by adding paraffinic solvents at the solvent/bitumen ratio (S/B ratio) above a critical value [2, 3], a phenomenon of significance for industrial processes. For instance, solids and water are removed from bitumen froth in paraffinic froth treatment (PFT) through dilution by paraffinic solvents [4]. For several years, numerous research has been done to recognize molecular or colloidal structures, solubility, and phase behaviour of asphaltene in different solvents and bitumen. Furthermore, asphaltene precipitation involves dynamic processes on multiple length scales (from nanometers to millimeters) and time scales (from seconds to days). However, dilution-induced asphaltene precipitation is still one of the most significant and challenging topics due to the complexity of the physical and chemical properties of asphaltene.

In parallel, dilution-induced liquid-liquid phase separation is omnipresent in many other technological or industrial processes. An example is the Ouzo effect in a ternary mixture of oil, ethanol, and water [5]. When water is added to a clear Greek alcoholic drink Ouzo, anise oils become oversaturated due to dilution and form nanodroplets spontaneously in the cloudy mixture [6]. The same effect can also be seen when eucalyptus disinfectants are diluted with water [7]. In liquid-liquid microextraction, oil microdroplets separated by dilution are the basic unit to concentrate and separate trace analytes from aqueous samples [8]. Gas molecules, lipids or polymers dissolved in a polar organic solvent all exhibit similar effects, forming bubbles or nanoparticles when diluted by a poor solvent. The process is also called solvent exchange [9], nanoprecipitation [10], solvent displacement, solvent shifting [11, 12], or flash precipitation.

Up to now, it has rarely been discussed that asphaltene precipitation shares several key features of dilution-induced formation of microdomains (droplets or nanoparticles) in aqueous systems via the ouzo effect. The phase separation appears as microphase separation rather than bulk phase separation, which means that the phase separation forms uniformly distributed droplets or particles. The size and distribution of microdomains are determined not only by the concentration of the compositions but also by the temporal and spatial characteristics of the mixing process of the solvents [5]. The addition of solvent greatly affects the size distribution, morphological characteristics, and physical and chemical properties of the formed microdomains. The formation and growth of microdomains are affected by several factors, including solution composition [19], mixing conditions of the solvent and the solution [5], and subsequent interactions with microdomains in proximity [20]. The dynamics of droplet formation via the ouzo effect have seldom been compared to the dynamics of asphaltene precipitation. The latest reviews on this subject are listed in Table 1. In this critical review, for the first time, we will draw a comparison between solvent-induced asphaltene

Table 1: Key existing review articles in the last two years.

Title	Subject of study	Year	Authors
Distributed Properties of Asphaltene Nano-aggregates in Crude Oils: A Review	Molecular properties of asphaltene, particle size distribution of nano-aggregates and their effect on asphaltene precipitation. Molecular weight of nano-aggregates varies, and can be up to 4,0000 Da. The aggregates may be smaller than 100 nm.	2021	Gray et al. [13]
Lab-on-a-Chip systems in asphaltene characterization: A review of recent advances	Research progress on asphaltene precipitation by microfluidic devices. The confinement in microfluidics may have effects on the rheological properties of crude oil.	2021	Mozaffari et al. [14]
Asphaltene precipitation and deposition: A critical review	Comparison of models of asphaltene deposition to surfaces with experimental results. Asphaltenes with different molecular structures may exhibit different deposition models, and controversy on asphaltene structure hinders development of a unified asphaltene precipitation model.	2021	Mohammed et al. [15]
A review on chemical sand production control techniques in oil reservoirs	Introduction and evaluation of methods for controlling and suppressing sand formation in oil reservoirs	2022	Saghandali et al. [16]
Crude oil oxidation in an air injection based enhanced oil recovery process: Chemical reaction mechanism and catalysis	Progress of air injection for heavy oil recovery, summarize the problems faced at the current stage and propose possible solutions	2022	Yuan et al. [17]
Perspectives on microfluidics for the study of asphaltenes in Upstream Hydrocarbon Production: A Minireview	Asphaltene deposition and emulsion stability in microfluidic channels. Small dimensions in microfluidic devices shortens analysis time, generating high-quality and reliable data for understanding of dynamic behavior.	2022	Sharma and Hartman [18]

precipitation and nanodroplet formation via the ouzo effect with emphasis on effects from mixing conditions.

2. Thermodynamics of solvent-induced droplet formation and asphaltene precipitation

2.1. Spontaneous droplet formation via ouzo effect

Ouzo effect is the basis for liquid-liquid microphase separation induced by dilution. Ouzo effect, also called spontaneous emulsification, is a milky oil-in-water emulsion obtained by adding water to an anise-flavoured spirit. Such emulsion is formed by minimal mixing and is stable for a long time [21–23]. Recently, the Ouzo effect has been seen as a technique for the large-scale generation of surfactant-free emulsion without mechanical agitation [24]. A standard Ouzo effect system consists of three parts: oil, non-solvent (i.e., water), and co-solvent (i.e. ethanol). A typical phase diagram of the ternary system is shown in Figure 1 [19, 25, 26]. The spontaneous formation of microdomains takes place not only for liquid droplets in the case of the ouzo effect but also for polymer or nanoparticles, where the process is often referred to as nanoprecipitation [10].

Oil is miscible with ethanol but immiscible with water. The ternary solution is a homogeneous solution with the composition above the binodal curve. With the addition of water, the oil solubility decreases, leading to oil oversaturation to form a new phase when the composition is below the binodal curve. The Ouzo region is a metastable region in which the Gibbs free energy is not a minimum, but there is a large kinetic barrier for phase separation, resulting in a stable emulsion[6]. In this process, the total volume of droplets generated is determined by the phase diagram, and the final volume of droplets increases with the oil concentration [12].

2.2. Asphaltene precipitation induced by diluents

As the phase separation process can be triggered by the addition of non-solvents, the physico and hydrodynamical aspects of dilution-induced asphaltene precipitation are similar to the droplet formation caused by ouzo effect. In the asphaltene precipitation process, as shown in Figure 2, a few molecules first form nano-aggregates through self-association [28]. Then, nano-aggregates form particles or flocs revealed as phase separation. The onset and quantity of asphaltene precipitation are related to the solvent type, S/B ratio, temperature, and pressure [1, 29]. Yen-Mullins model proposed that there was a cluster state ($\sim 5\text{ nm}$) between nano-aggregates and phase separation states [30]. The asphaltene aggregation process consists of π - π bonding between PAHs as well as other molecular interactions such as hydrogen bonding and acid-base interactions [31, 32]. After the formation of the nano-aggregates, steric repulsion restricts adding more molecules [28].

In aromatic-based solutions, asphaltene colloids are in a favourable liquid environment, leading to the swelling and extended structures of asphaltene colloids. The asphaltene colloids repel each other due to the

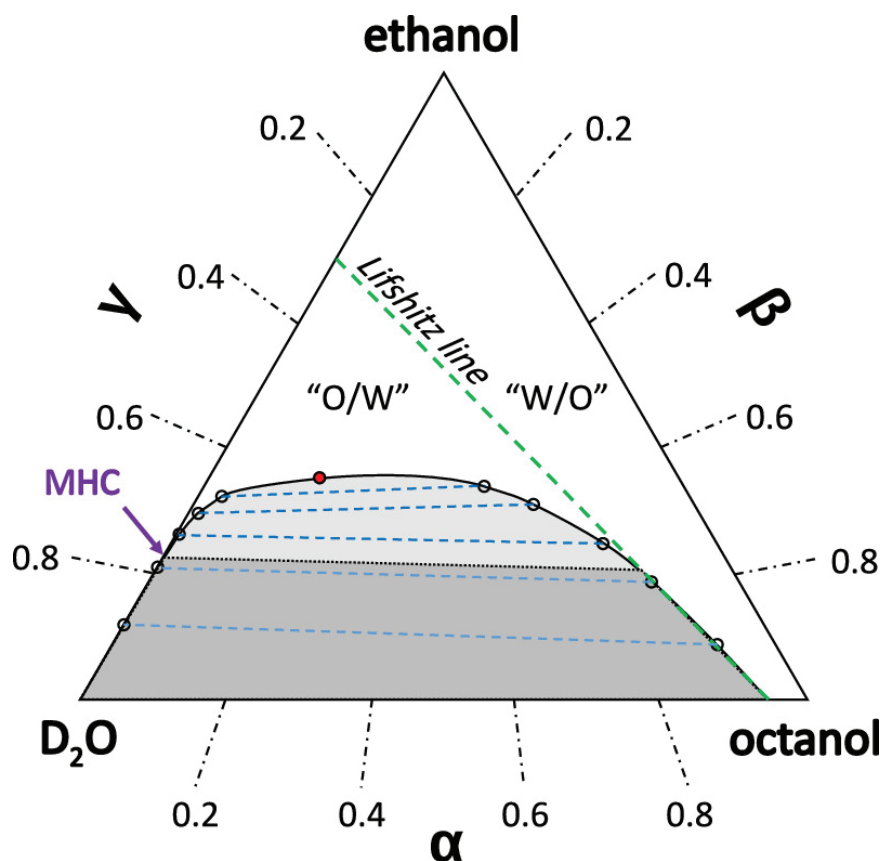


Figure 1: Representative solubility phase diagram of the ternary system of oil, ethanol, and heavy water. Where α , β , and γ are the mass fractions. Figure 1 Reproduced with permission from ref [27]. Copyright 2021 American Chemical Society.

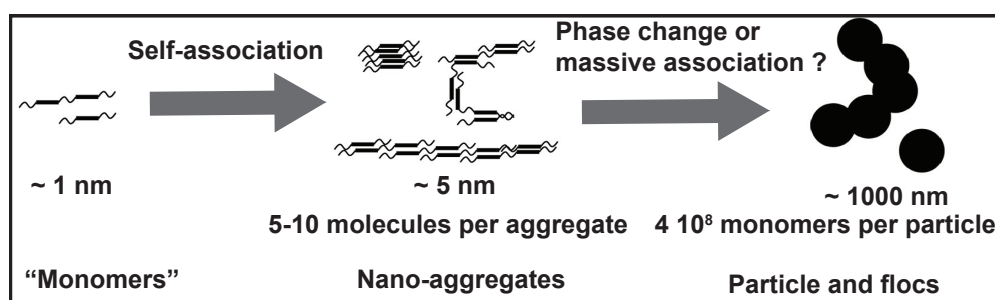


Figure 2: Molecular, nano-aggregate, and precipitate length scales of asphaltene. Figure 2 Reproduced with permission from ref [28]. Copyright 2013 American Chemical Society.

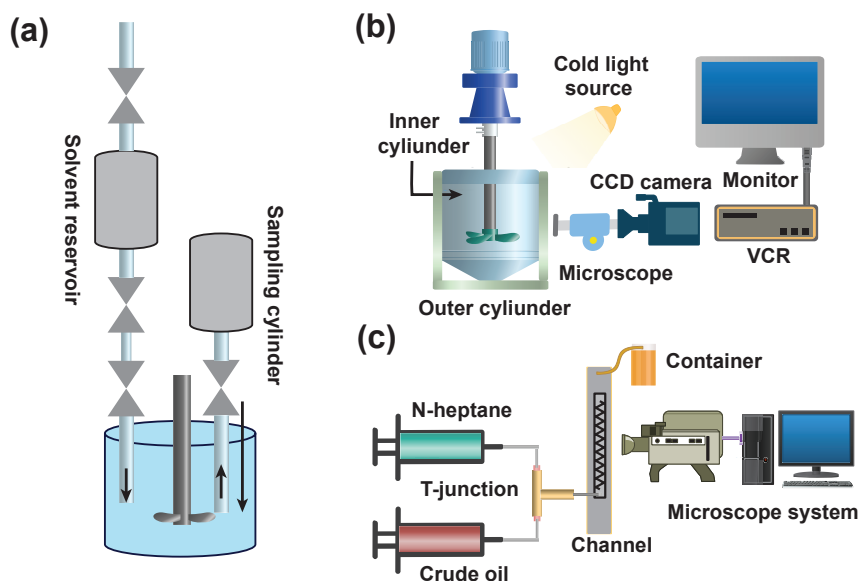


Figure 3: Standard apparatus for asphaltene precipitation studies: (a) Bulk mixing system, (b) constant shear rate system, and (c) co-injection system. Panel (a) reproduced with permission from ref [3]. Copyright 2017 American Chemical Society; Panel (b) reproduced with permission from ref [38]. Copyright 2003 John Wiley & Sons, Inc.; Panel (c) reproduced with permission from ref [39]. Copyright 2016 Elsevier.

steric repulsion originating from the extended chains. In paraffinic-based solvents, the liquid surrounding becomes less favourable for stretching of the asphaltene colloids, resulting in the reduction of the steric repulsion. The van der Waals attraction leads the aggregation of the asphaltene colloids to grow to large particles [32–35].

The influence of the type of the precipitant on the asphaltene precipitation is due to the difference in Hildebrand solubility parameters, which is different for different types of *n*-alkanes [36]. The greater difference in the Hildebrand solubility parameters between solvent and asphaltene means the stronger attractive interaction between asphaltene particles [35]. In addition to *n*-alkanes, some other chemicals can also be used as a precipitant to induce asphaltene precipitation, such as carbon dioxide [37].

Xu [3] attributed the effects of the S/B ratio and type of the precipitant on asphaltene precipitation to differences in the Hildebrand solubility parameter (δ). As shown in Figure 5(a), the total asphaltene precipitation decreases with the increase of δ due to asphaltene becoming more soluble in the solvents.

Solvent/bitumen ratio (S/B ratio) is the mass ratio of the paraffinic solvent to bitumen. Asphaltene precipitation happens when the S/B ratio is higher than the onset. But the onset measured by different methods may not be the same. Tavakkoli et al. [40] found that the onset measured by indirect methods such as the near-infrared method (NIR) is lower than that obtained from a direct method such as microscopy. This phenomenon is because different sizes of the smallest particles are observed by different methods. When

the equipment was able to detect smaller particles, the measured S/B ratio would be smaller.

Several researchers found that the rate of asphaltene precipitation increases with the increase of the S/B ratio in terms of the yield and size of asphaltene [41, 42]. The interaction between asphaltene particles is stronger at a higher S/B ratio, resulting in higher rates of asphaltene precipitation and aggregation [35]. However, it is also reported that the change in the interaction between asphaltene particles also leads to a noteworthy change in the mechanism of asphaltene aggregation from diffusion-limited aggregation (DLA) to reaction-limited aggregation (RLA), particularly with the decrease in the S/B ratio [43, 44]. Two classical models were applied to describe the growth dynamics based on the mean diameter of the precipitates: diffusion-limited aggregation (DLA) and reaction-limited aggregation (RLA) [44, 45]. Although the mechanism of this transition was not fully understood, transitions from one model to another were observed at different S/B ratios, [44–46].

3. Effects of mixing conditions on asphaltene precipitation

Different from varying the characteristics of precipitates by mixture composition, the mixing dynamics in addition of the poor solvent may impact on the total amount and size distribution of the generated droplets or particles without changing the ratio of the antisolvent, due to the non-equilibrium nature before the homogeneous mixture is achieved. It is known that mixing conditions significantly impact the Ouzo effect from nucleation to the growth of the droplets. Johnson and Prudhomme [47] work reported that faster mixing resulted in a reduction in nanoparticle size induced by the ouzo effect. Zhao et al. [48] also reported that the particle size decreased with the increase of the speed of rotating by changing the agitator speed. Beck-Broichsitter [49] work described when the ratio of solvent/non-solvent increased, and the precipitation was more sufficient, finally leading to the generation of smaller nanoparticles. The effect of mixing conditions on the Ouzo effect is attributed to the timescale required for the system to reach homogeneous mixing, before which the local oversaturation varies with time.

The effect of mixing dynamics on dilution-induced liquid-liquid phase separation has been extensively studied [24]. Many hydrodynamic factors of the mixing process affect the morphology of the resulting droplet, including flow rate [5], diffusion coefficient [50], viscosity [51], and profile of the flow [52]. The mixing dynamics also affect the asphaltene precipitation, considering the similarity of these two processes.

3.1. Shear rate in a mixing tank

Previous studies on asphaltene precipitation mainly focused on the influence of thermodynamic factors, including S/B ratio [53], type of the precipitant [54], and temperature [55]. As represented in Figure 3(a), a bulk mixing system was used. Results from the bulk mixture on asphaltene precipitation were studied as summarized in Table 2.

Table 2: Asphaltene precipitation in bulk by mixing.

Mixing mechanism	Oil	Solvent	Reference
Agitator	Venezuela bitumen	n-Heptane	[56]
	Crude oil	n-Heptane	[57]
	McMurray bitumen froth	n-Pentane, isopentane, neopentane	[3]
	Athabasca bitumen froth	n-Pentane, n-Hexane, n-Heptane	[58]
Hand shaken	Crude oil	n-Heptane	[59]
	Caoqiao crude oil	C5 -C12	[60]
Pour into	Karazhanbas crude oil	n-Heptane	[44]
	Maya crude oil, Cold lake bitumen	C5 -C16	[61]
Sonicated	Cold lake bitumen	n-Heptane, n-Pentane, n-Hexane, n-Octane	[42]

The mixing dynamics affects the movement of particles, which leads to the difference in particle collision frequency and in the formation of particles from nano-aggregates in Figure 2. The collision frequency is determined by the movement of the particles, as shown in Equation (1). Mechanical shearing of the mixture of crude oil and diluent significantly influences the settling properties of the aggregates and the size distribution of asphaltene precipitates. Large asphaltene-solid aggregates with high density formed when solvent and bitumen froth was mixed at a higher speed for a long time [62]. Rahmani et al. [63] controlled the shear rate in a bulk system by rotating the rate of a cylinder, as shown in Figure 3(b). Under the action of shear rate, asphaltene precipitation is an equilibrium between aggregation and fragmentation processes. The shear rate intensified the movement of asphaltene particles, enhancing the collision frequency [38].

The difference in the settling rate of asphaltene particles also induces the collision of asphaltene particles. As a result, three factors contribute to the collision frequency of the system in Figure 3(b), including

Brownian motion, shear rate, and differential settling of asphaltene particles [64].

$$\text{Brownian} : \alpha_{i,j} = \frac{2}{3} \frac{RT}{\mu} \frac{(d_i + d_j)^2}{d_i d_j} \quad (1a)$$

$$\text{Shear} : \alpha_{i,j} = \frac{G}{6} (d_i + d_j)^3 \quad (1b)$$

$$\text{Settling} : \alpha_{i,j} = \frac{\pi g}{72\mu} (d_i + d_j)^2 |\Delta\rho_i d_i^2 - \Delta\rho_j d_j^2| \quad (1c)$$

where $\alpha_{i,j}$ is collision frequency, R is ideal gas constant, μ is viscosity, T is temperature, G is shear stress, d_i and d_j are the diameter of particle i and j , respectively, ρ_i and ρ_j are the density of particle i and j , respectively.

The pressure imbalance between the two sides of the asphaltene particles caused by the shear rate also causes the fragmentation [65]. Fragmentation results in the change of large particles into small particles, which limits the growth of particle size [66]. Considering collision and fragmentation, the growth of asphaltene particles can be calculated by the Smoluchowski aggregation model [64]:

$$\frac{dn_k}{dt} = \frac{1}{2} \sum_{i+j=k} \alpha_{i,j} \beta_{i,j} n_i n_j - n_k \sum_{i \geq 1} \alpha_{i,k} \beta_{i,k} n_i - B_k n_k + \sum_{j=k+1}^{n_{max}} \gamma_{k,j} B_j n_j \quad (2)$$

where t is time, n_k is the number density of particles of size k , $\beta_{i,j}$ is the collision efficiency, which depends on the interaction between asphaltene particles in the solvents, B_k and B_j are the fragmentation rate of particles k and j , n_{max} is the largest particle size form fragments of size k by breakage, $\gamma_{k,j}$ is the volume fraction of the fragments of size i originating from size j particles. The fragmentation rate (B_k) is a function of particle volume (V_k) [67, 68]:

$$B_k = b V_k^{1/3} \quad (3)$$

where b is a correlation parameter [64].

The existence of shear rate enhances aggregation and fragmentation of asphaltene particles simultaneously [69]. At the beginning of mixing of asphaltene solution and the paraffinic solvents, the aggregation dominates the process, leading to the size increase of asphaltene particles until a critical value. The fragmentation then dominates the process, resulting in the size decreases. At the final state, aggregation and fragmentation reach an equilibrium, and the size of asphaltene particles remains stable [38]. With the increase in shear rate, the rate of aggregation of asphaltene particles becomes faster, but the rate of fragmentation also increases. Therefore, the size of asphaltene particles at the final state decreases with the increase of shear rate, as shown in Figure 5(b) [64]. The precipitation dynamics of asphaltene particles are the same at all points in the system, as shown in Figure 5(c). Therefore, the local composition does not affect asphaltene precipitation in the constant shear rate system.

3.2. Mixing in a narrow channel

Microfluidics has become a powerful approach for the reproducible synthesis of nanomaterials by nanoprecipitation. Microfluidics offers the possibility to produce nanoparticles in a continuous flow, facilitating high-quality synthesis of large amounts. In addition, it could be further scaled-up through parallel fabrication. The dynamics of phase separation can be achieved by co-injection of a mixture of oil, a good solvent and a poor solvent into a narrow channel. Chen et al. [70] found that for the channel of cross-shaped, an increase in flow rate leads to an increase in nanoparticle size. However, for the channel of multi-lamination, the increase in flow velocity leads to a decrease in nanoparticle size. In the split-recombine channel, the flow rate has almost no effect on the particle size. Using COMSOL simulation, Zhao et al. [48] found that the influence of flow velocity change on the dynamics of precipitation was due to the difference in solution mixing. Faster mixing results in smaller droplets or particles. For channels with different dimensions, the effect of flow rate on solution mixing is different. Therefore, the influence of flow velocity change on precipitation kinetics in different channels is different [71]. To show the importance of controlling the mixing conditions for polymer nanoparticles loaded with a fluorescence dye and identify the optimal microfluidic setup for the production of polymer nanoparticles for biomedical applications, Chen et al. [70] compared the size and fluorescence properties of synthesized nanoparticles by using 5 different microfluidic mixers. The flow rate significantly impacted the nanoparticles' size and fluorescence properties. Impact jet mixers strongly decrease the size of nanoparticles due to strong enhancement in the mixing speed. The mixing speed also has an effect on the enhancement of the fluorescence properties of the nanoparticles.

Co-injection is a method for the study of asphaltene precipitation under different flow conditions. The mechanism is shown in Figure 3(c). Asphaltene solution and the precipitant are injected from two syringes into a microcapillary. The asphaltene precipitation happens when mixing the asphaltene solution and the precipitant is well enough. The flow rate and chemical composition in the two syringes can be controlled. The microcapillary tube can be changed to substrates with different types of patterns to investigate the structure effect. Some typical studies are summarized in Table 3.

Boek et al. [72, 74] measured the conductivity change of the microcapillary in the co-injection process. The more conductivity decreases for a given time means, the higher rate of asphaltene deposition. They found that the increase in the injection rate of the solutions accelerates the deposition rate of asphaltene initially. But the microcapillary is not blocked by the asphaltene deposition at a higher flow rate ($10 \mu\text{L}/\text{min}$) because the deposits are removed by the flow. Using the same setup, [39, 75] found that the thickness of the asphaltene deposition layer increased with the flow rate from $10 \mu\text{L}/\text{min}$ to $40 \mu\text{L}/\text{min}$ and then decreased from $40 \mu\text{L}/\text{min}$ to $100 \mu\text{L}/\text{min}$. The results were verified by Zhuang et al. [75] using a 3D microscope. Later, by using the microscope to visualize the asphaltene particles, Li et al. [41] found that the size of the asphaltene particles increases with the increase of the flow rate of injection of the solutions, as shown in Figure 5(d).

Table 3: Co-injection for mixing to induce asphaltene precipitation by n-heptane.

Mixing device	Oil	Reference
Co-injection into a microcapillary	C7 asphaltene in toluene	Boek et al. [72]
	South America heavy oil	Lawal et al. [73]
	Venezuela crude oil	Li et al. [41]
	Crude oil	Boek et al. [74], Zhuang et al. [39, 75]
Co-injection into a microchannel with micropatterns	C7 asphaltene in toluene	Lin et al. [76]
		Hu et al. [77]
	C5 asphaltene in toluene	Lin et al. [78]
		Lin et al. [79]
n-Heptane flux mixes with model oil in cavity	Asphaltene in benzene	Shalygin et al. [80]

Li et al. [56] followed asphaltene aggregation and deposition on a microcapillary tube for the purpose of mimicking the situation in a porous medium. A faster flow rate was found to lead to larger asphaltene precipitates on the wall of the capillary tube [41]. But Lawal et al. [73] reported that the deposition of asphaltene was independent of flow rate and was reasonably uniform along the capillary tube, in disagreement with earlier observation. The above-reported effects from mixing after the solvent addition were attributed to interruption of the fractal structures of asphaltene precipitates or aggregate formation. There may also be effects from precipitate-flow interactions or interactions among precipitates in the mixing flow. The deposition on the microcapillary tube may be influenced by both asphaltene phase separation and different precipitates-wall under the shear along the tube. Furthermore, it is unknown how water drops influence the onset of asphaltene precipitation and their association with precipitates under mixing processes.

Hu et al. [77] changed the microcapillary into a channel with porous structures. They found that the pores were easier to block when the solutions' injection rate was low. Lin et al. [76, 78] found that the asphaltene deposits tended to grow against the flow direction rather than laterally because a high shear rate limited the growth of asphaltene, regardless of whether using a dispersant (Figure 4(a)). The smaller asphaltene particles were easier to resist the shear from the flow [79]. And Lin et al. [83] found that asphaltene preferred to precipitate in the large pores rather than small pores. Qi et al. [81] found that small pores were easier to block than large ones, as shown in Figure 4(b). Keshmiri et al. [82] changed the hydrophobicity of the surface and found that deposition of asphaltene on a hydrophilic surface is faster (Figure 4(c)), which is caused by the higher interaction potential between asphaltene and hydrophilic surface.

Shalygin et al. [80] found that the different flow affects the mixing and ultimately changes the local chemical composition so that the asphaltene precipitation in different positions in the substrate may be different.

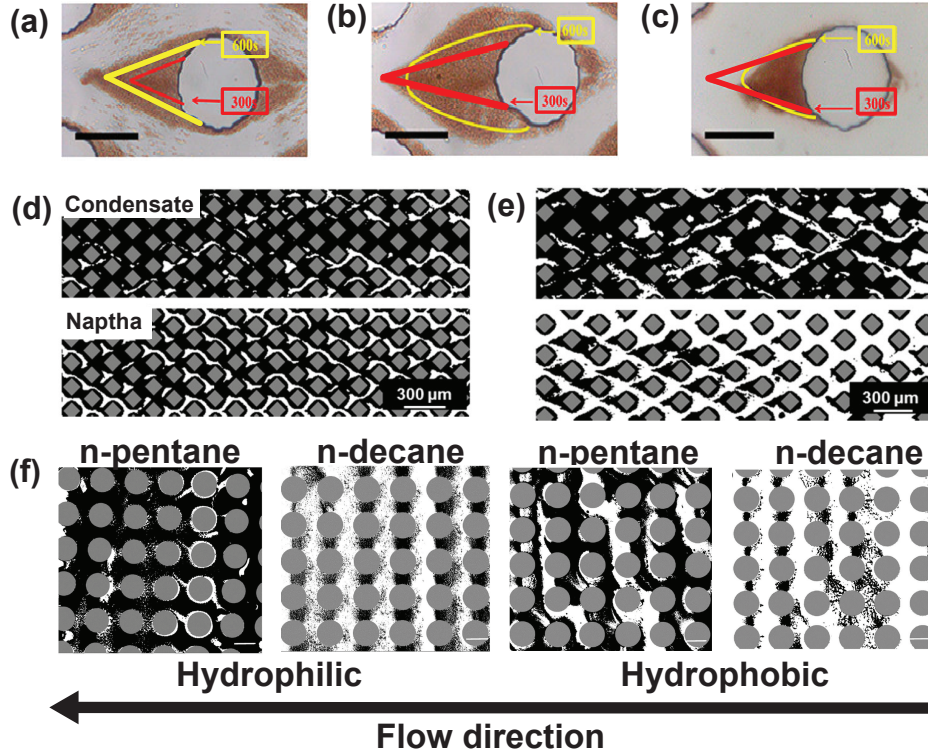


Figure 4: Asphaltene deposition growth in different dispersants: (a) without dispersants, (b) with p-octylphenol, and (c) with iso-dodecylphenol. Deposition profiles of asphaltene in condensate and naphtha for (d) 50 μm and (e) 100 μm pore throat. (f) Deposition profiles of asphaltene in hydrophilic and hydrophobic surfaces. Panels (a)-(c) reproduced with permission from ref [79]. Copyright 2018 American Chemical Society; Panels (d)-(e) reproduced with permission from ref [81]. Copyright 2017 American Chemical Society; Panel (f) reproduced with permission from ref [82]. Copyright 2018 Elsevier.

Mokhtari et al. [84] also found that the higher local concentration of asphaltene at the water-oil interface can accelerate the aggregation rate of asphaltene particles, ultimately enhancing asphaltene precipitation. Therefore, mixing dynamics not only affect particle movement and change particle collision frequency but also affect the local chemical composition and change the collision efficiency of asphaltene particles.

4. Droplet formation and asphaltene precipitation from diffusive-dominated mixing

4.1. Liquid-liquid separation via ouzo effect in confined spaces

Diffusive-dominated mixing is a well-controlled method to study the influence of mixing parameters on phase separation process. The experiment is more reproducible and the process is easier to be described by modelling. A series of publications from Lu et al. [85] reported that in ternary liquid-liquid systems, the

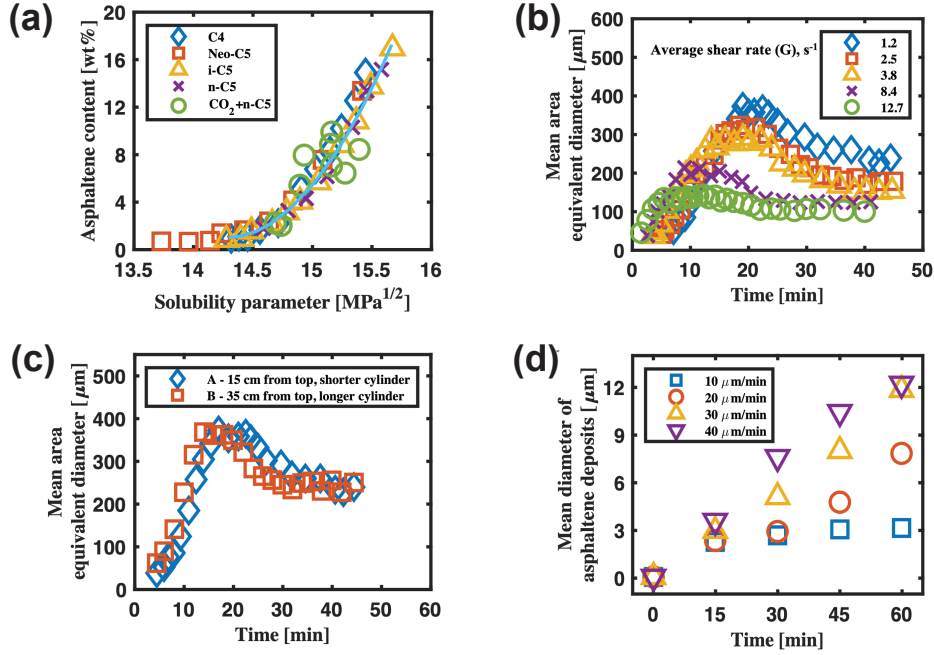


Figure 5: (a) Relationship between asphaltene residues in bitumen with Hildebrand Solubility parameter in a bulk mixing system. (b) Growth kinetics of asphaltene particles under different shear rates and (c) comparison between different locations in a constant shear rate system. (d) Growth kinetics comparison of asphaltene induced by different flow rates in a co-injection system. Panel (a) reproduced with permission from ref [3]. Copyright 2018 American Chemical Society; Panels (b) and (c) are reproduced with permission from ref [38]. Copyright 2003 John Wiley & Sons, Inc.; Panel (d) reproduced with permission from ref [41]. Copyright 2018 Elsevier.

oversaturation level and growth duration of the new phase are mediated by Péclet number (Equation 4) of the flow, geometrical features of the fluid chamber, and the solution composition. A faster laminar flow of the solvent leads to larger droplets from the phase separation. The complex effects from solvent diffusion and mixing dynamics were decoupled for microphase separation in a confined 2-dimensional channel.

As sketched in Figure 6, the horizontal rectangular flow chamber was constructed by assembling two glass plates sealed with a spacer. The distance from the top plate to the bottom surface is very close (i.e., $20 \mu\text{m}$) to avoid convective flow. The main flow chamber is flanked by two deep side channels (i.e., $260 \mu\text{m}$), as indicated by the two rectangles in the sketch [87]. Inside the quasi-2D fluid chamber, the concentration of the solvent was known both space-wise and time-wise [85]. In the study of the liquid-liquid separation, diffusive-dominated mixing causes the branch-like the structure of droplets, as shown in Figure [85], as shown in Figure 7(a). Arends et al. [88, 89] found a jetting phenomenon of the droplets, and the speed of the jetting was related to the composition of the solution. Meng et al. [87] successfully applied the proposed

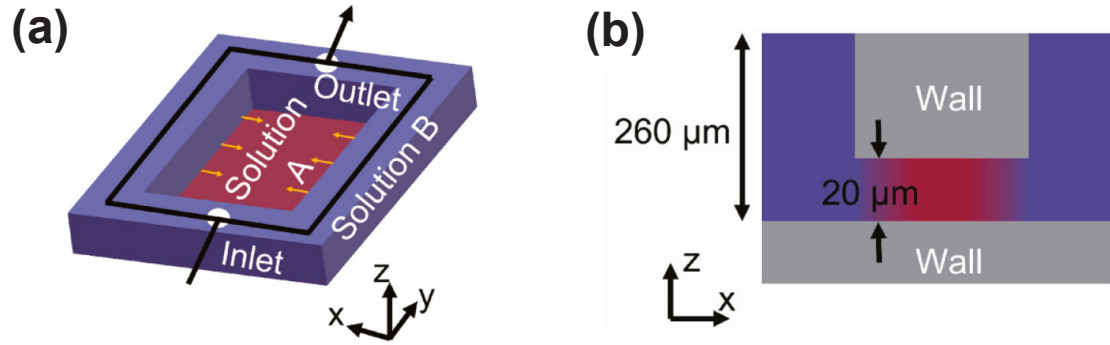


Figure 6: (a) Sketch of the quasi-2D microchamber used in this study. The black arrow indicates the flow direction of the poor solvent. Yellow arrows indicate the diffusion direction of the poor solvent. (b) Side view of the cross-section of the microchamber. Panels (a) and (b) are reproduced with permission from ref [86]. Copyright 2022 Elsevier.

quasi-2D chamber to the study of liquid–solid separation systems such as oiling–out crystallization, as shown in Figure 7(b).

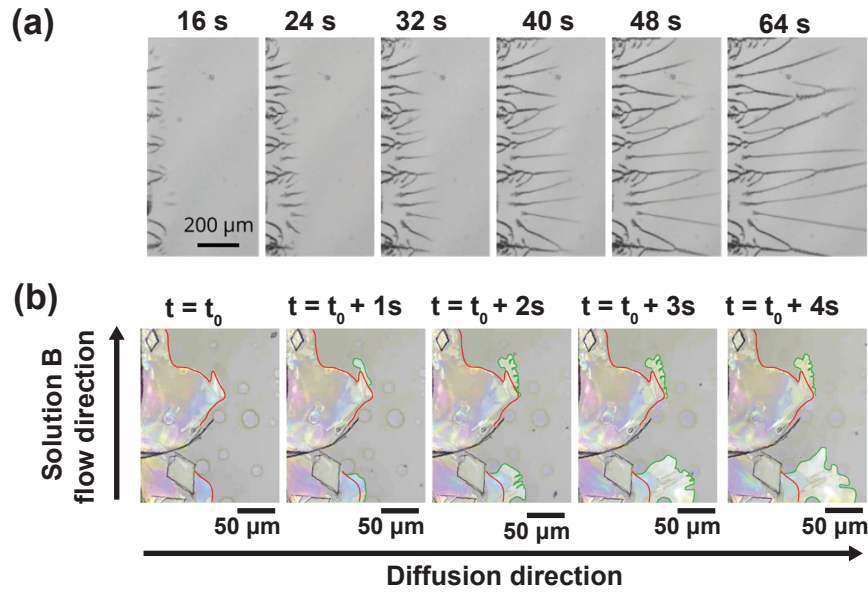


Figure 7: (a) Growth of branch structure of precipitations and (b) crystallization in the quasi-2D chamber. Panel (a) reproduced with permission from ref [85]. Copyright 2017 National Academy of Sciences; Panel (b) reproduced with permission from ref [87]. Copyright 2021 Springer Nature.

4.2. Visualization of asphaltene precipitation from diffusive-dominated mixing

Inspired by the phenomenon in the quasi-2D chamber, Meng et al. [87] used the quasi-2D chamber to study the precipitation of asphaltene caused by dilution. Unlike the traditional bulk system, [90, 91], asphaltene precipitation in the diffusive-dominated mixture system is not a continuous process. As shown in Figure 9(a), for a specific position in the main channel, the solution composition gradually changed from pure asphaltene solution to pure n-pentane, and asphaltene precipitation began at the moment that the n-pentane concentration was higher than that of onset until asphaltene solution was totally displaced by n-pentane. This process freezes the process of the early stage of asphaltene precipitation.

Direct visualization of the asphaltene precipitates from an early stage is challenging, including size distribution and structural characteristics, mainly because of the high optical density of the mixture of asphaltene components [92]. Confocal laser-scanning microscopy in a transmission mode was recently used as high-spatial-resolution measurements [46]. The size distribution of asphaltene particles in different solvents was observed versus time when a very thin film of the mixture was confined between two plates [46]. Confocal microscopy and image processing techniques were used to study the yield and size distribution of asphaltene particles after phase separation [93, 94]. In the above-mentioned optical measurements, the concentration of asphaltene must remain very low ($< 0.2 \text{ mg/mL}$) to allow enough intensity of the light passing through the samples [1]. Therefore, the measurements were either much lower than the concentration regimes in bitumen or the entire early stage dynamics of the precipitation were missed due to the high solvent ratio above the critical ratio.

Total internal reflection fluorescence microscopic system (TIRF) in Figure 8(a) is a powerful technique to overcome experimental difficulties from asphaltene while providing high temporal and spatial resolutions [95]. In the configuration of TIRF, the light propagates within the substrate by total internal reflection and generates an evanescent field from the substrate [95]. The selective excitation and visualization of samples in TIRF are confined in the evanescent field generated from the total internal reflection. The thickness of the evanescent field is approximately 200 nm adjacent to a substrate, depending on the incident angle and refractive index of the media [96]. Compared with a transmission or reflection mode of the conventional optical microscope, the most desirable feature of the TIRF configuration is that the high scattering background from the medium far from the substrate can be largely neglected [97]. Therefore, the difficulty of the high optical density will be largely overcome. The unique capacity of TIRF allows for tracking the microphase separation during solvent mixing [98].

There are interesting insights obtained from combining diffusive mixing with TRIF measurements. At the early stage of asphaltene precipitation, two types of asphaltene particles are formed, including individually existing particles and fractal aggregates, as shown in Figure 9(b). With image processing, the fractal aggregates can be separated into isolated particles (Figure 9(c)). The size of the isolated particles is comparable with the individually existing particles, and the size is always between 0.2 and $0.4 \text{ }\mu\text{m}$ (Figure

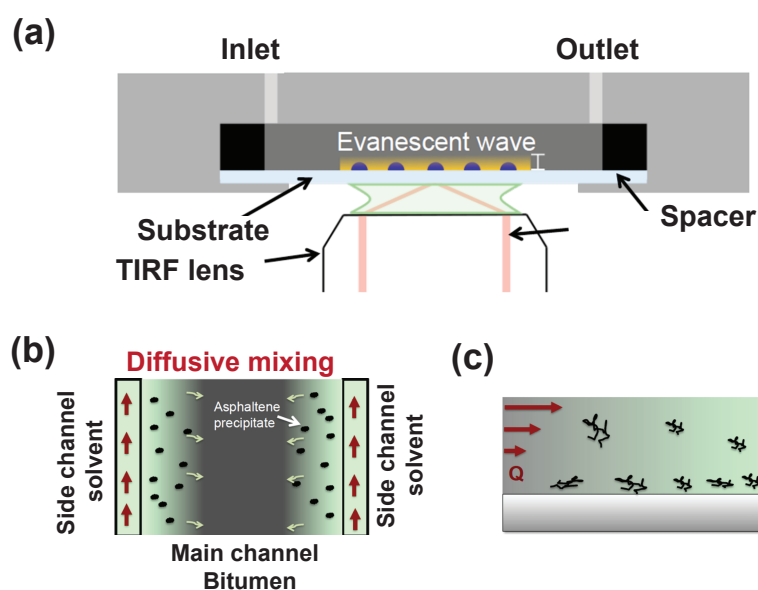


Figure 8: (a) Sketch of the total internal reflection fluorescence microscopic system (TIRF) with the designed microfluidic chamber. (b) A quasi-2D channel for diffusion driven mixing. The channel has two deep-side subchannels (in two rectangular boxes) and a very narrow main channel. (c) Sketch of the substrates for asphaltene precipitation on a planar surface [5, 87]. Panel (a) reproduced with permission from ref [97]. Copyright 2018 The Royal Society of Chemistry.

9(d)). Therefore, the particles from 0.2 to 0.4 μm are defined as primary submicron particles (PSMPs), which means they are the basic blocking units for fractal aggregates in the asphaltene precipitation process. PSMPs are always formed in the studies of Meng et al. [86, 99], including different solvent concentrations and mixing conditions, and whether nonylphenol is used as inhibitor, as summarized in Table 4.

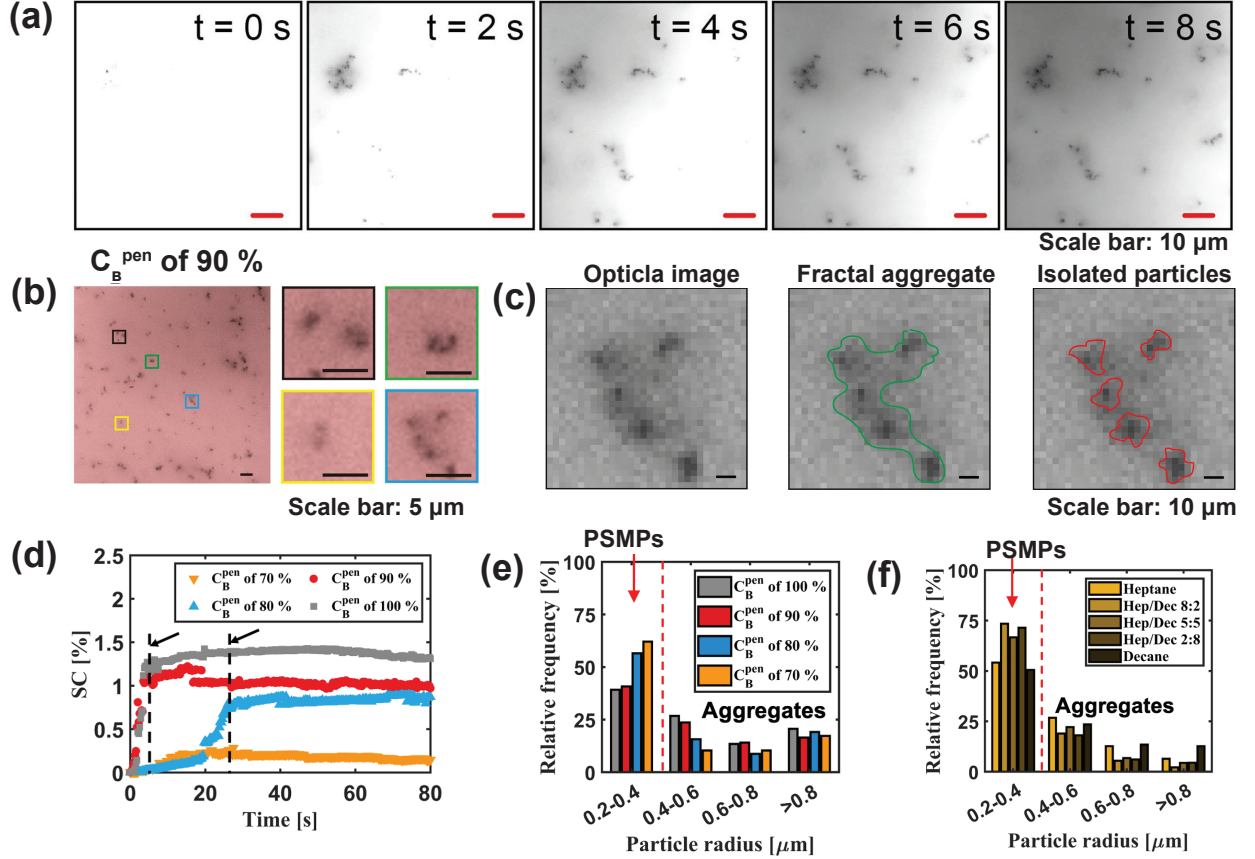


Figure 9: (a) Snapshots of the growth dynamics of the asphaltene particles in the quasi-2D chamber. (b) Morphology of asphaltene particles at the final state. (c) Image analysis to separate the aggregates into isolated particles. (d) Growth dynamics of the surface coverage of asphaltene particles in the quasi-2D chamber. Size distribution of the asphaltene particles precipitated by (e) n-pentane and (f) a mixture of n-heptane and n-decane. Panels (a)-(e) are reproduced with permission from ref [99]. Copyright 2021 Elsevier; Panel (f) reproduced with permission from ref [86]. Copyright 2022 Elsevier.

The yield and size distribution of the asphaltene particles depends on the Hildebrand solubility parameter of the paraffinic solvent and the diffusion coefficient. Hildebrand solubility parameter represents the interaction between compounds. The closer the Hildebrand solubility parameters are, the more likely that

the two compounds are miscible [36]. The diffusion coefficient affects the duration of the mixing, ultimately affecting the dynamics of asphaltene precipitation [86]. Therefore, the relative frequency of the PSMPs in different types of precipitants is different.

5. Droplet formation and asphaltene precipitation by solvent exchange

5.1. Flow rate during the solvent exchange

5.1.1. Effects of flow rate on droplet formation

Zeng et al. [100] proposed a device to control convective mixing: Solvent exchange [5, 101–105]. Solvent exchange is an effective approach to control the volume, composition, and size distribution of the final surface nanodroplets [106].

Figure 8(c) shows the sketch of solvent exchange. An increase in flow rate results in an increase in the size of the nanodroplets, as shown in Figure 10(a) [5]. The experimental data shows a scaling relationship between the total volume of the nanodroplets (Vol_f) and the Péclet number (Pe) of the flow (Figure 10(b)(c)). Pe is defined as the ratio between advective transport rate to diffusive transport rate and can be calculated by:

$$Pe = \frac{Q}{wD} \quad (4)$$

where Q is the flow rate, w is the width of the channel, and D is the diffusion coefficient. The scaling law is:

$$Vol_f \sim R_f^3 \sim h^3 Pe^{3/4} \quad (5)$$

where R_f is the final radius of the droplets, h is the channel height. The scaling law of $Pe^{3/4}$ is derived according to the diffusive growth of the droplets from the oversaturated droplet liquid transported by an external laminar flow.

5.1.2. Effect of flow rate on asphaltene precipitation

Inspired by the influence of the mixing conditions in the liquid–liquid phase separation process, Meng et al. [108] used microfluidic devices to control the mixing of a model oil and paraffinic solvents to study dilution-induced asphaltene precipitation. Asphaltene solution prefills the channel initially. Then precipitant is injected to displace the asphaltene solution, and the asphaltene precipitation happens simultaneously in this displacing process [5]. Different from the liquid–liquid phase separation, the scaling law of total volume to Pe in Equation (5) does not hold for the system of asphaltene precipitation, as shown in Figure 11(a)(b). COMSOL shows that n-heptane is concentrated at the top of the channel due to the large density difference between n-heptane and toluene. n-Heptane concentration at the bottom is always very low near the substrate due to the density difference between n-heptane and toluene, and this may be the reason that surface coverage of the asphaltene particles is not influenced by Pe (Figure 11(d)).

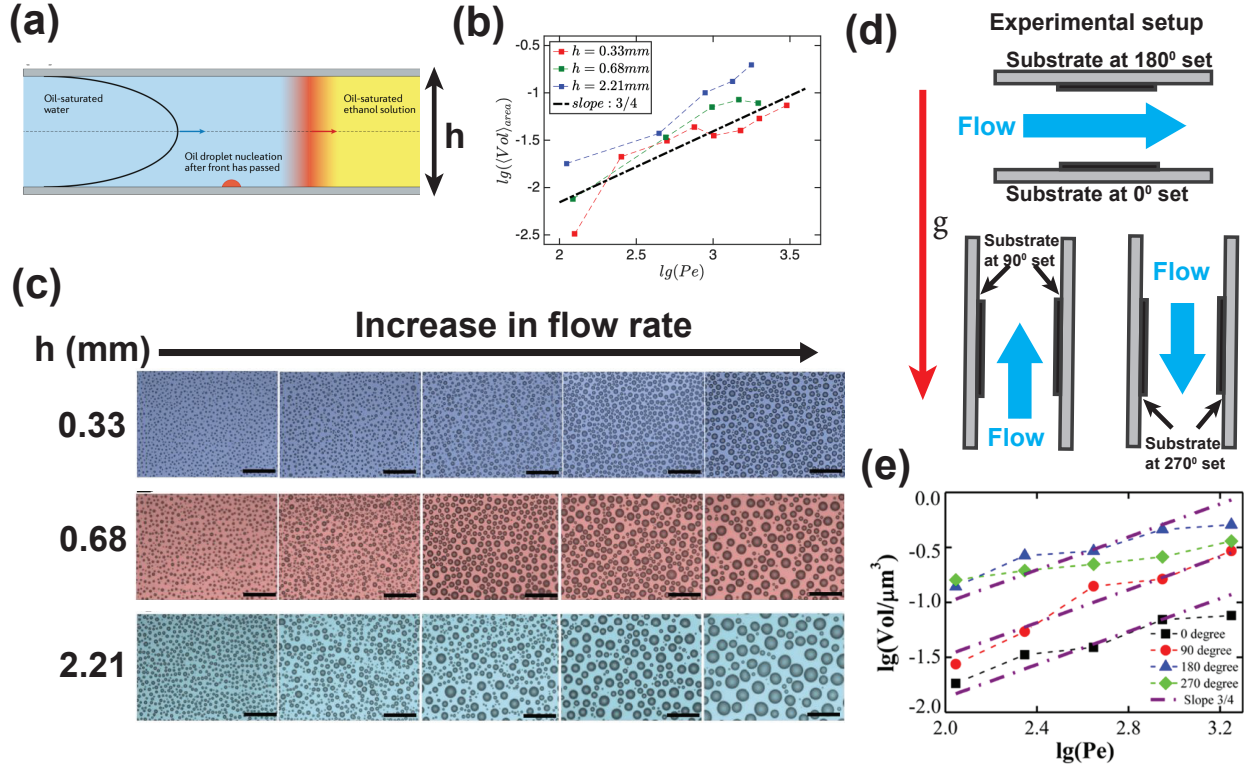


Figure 10: (a) Sketch for the solvent exchange. (b) Scaling law of Péclet number and total volume of the surface nanodroplets. (c) Snapshots of the nanodroplets formation under different Pe and channel heights. (d) Different orientations for solvent exchange. (e) Effect of orientation on the total volume of the surface nanodroplets. Panel (a) reproduced with permission from ref [107]. copyright 2020, Springer Nature Limited; Panels (b) and (c) are reproduced with permission from ref [5]. Copyright 2015 National Academy of Sciences; Panels (d) and (e) are reproduced with permission from ref [52]. Copyright 2015 American Chemical Society.

In addition, the size of the asphaltene particles decreases with the increase of Pe (Figure 11(c)). Abbas Rizvi et al. [109] also found that the size of the asphaltene particles deposited on the surface decreases with the increase of shear rates due to the breakage of asphaltene aggregates.

Elkhatib et al. [110] split the asphaltene particles into four classes, including nano-aggregates (1.5–4 nm), small clusters (SCs, 4–10 nm), medium clusters (MCs, 10–20 nm), large clusters (LCs, 20–100 nm), and extra-large clusters (XLCs, > 100 nm). Among them, LCs and XLCs are more easily to be removed from the surface by inertia forces originating from the flow. Sarsito et al. [111] found the deposition of asphaltene on the different surfaces may be different due to the hydrophobicity. Therefore, changes in flow

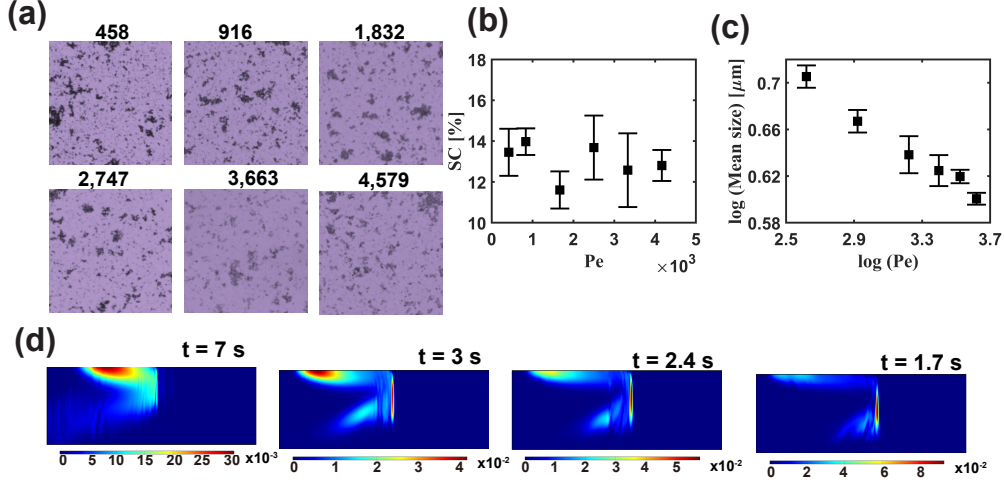


Figure 11: (a) Snapshots of the asphaltene particles precipitated under different Pe . Relationship of (b) surface coverage and (c) size with Pe . (d) COMSOL simulation to show the flow profile at different Pe [108]. Panels (a)-(d) are reproduced with permission from ref [108]. Copyright 2020 Elsevier.

rate affect not only asphaltene precipitation but also asphaltene deposition.

5.2. Effects of dimension and orientation of the channel

5.2.1. Effects on droplet formation

From Equation (5), for the same Pe , the total volume of the nanodroplets increases with the channel height. When the channel height is larger, the distance from the substrate to the position of the maximum flow velocity is longer due to the parabolic flow. Therefore, the duration of the oversaturation pulse is longer, resulting in a larger volume of nanodroplets. Meng et al. [108] observed a similar phenomenon in the asphaltene system. The surface coverage increases with the Rayleigh number (Ra), which is calculated by $Ra \sim h^3$ (Figure 12(a)). The COMSOL simulation visualized enhanced mixing from a larger channel height (Figure 12(b)(c)).

When the parabolic shape of the flow deforms, the distance between the walls to the position of the maximum flow rate varies when the density difference of solutions of A and B is significant enough. This distance variance only happens when the flow direction is perpendicular to gravity. The distance between the wall and the maximum flow point is not affected by gravity when the flow direction is parallel to the gravity direction, as shown in Figure 10(d) [52].

Yu et al. [52] placed the device of solvent exchange horizontally and vertically, and they found that the scaling law of Pe and Vol_f is still valid. However, under the conditions of the same Pe and channel height, due to the deformation of the parabolic profile, the volume of the nanodroplets of the 180° was higher than

180° and 0° when the density of solution B was higher than solution A (Figure 10(e)). In addition to the volume, the size distribution of the nanodroplets was also changed by varying the orientation [52].

For the horizontally placed device, if the deformation of the parabolic profile happens can be determined by Archimedes' number (Ar) of the system, which is calculated by:

$$Ar = \frac{gh^3}{\nu^2} \frac{\Delta\rho}{\rho} \quad (6)$$

where g is the gravity constant, ν is the kinematic viscosity, ρ , and $\Delta\rho$ are the density of solution B and the density difference between solutions of A and B, respectively. Gravitational effect plays a predominated role when $Ar \gg 1$. Therefore, the orientation effect only occurs when the channel height is high enough.

Zhang et al. [5] found that the increase in height led to an increase in the duration of the oversaturation pulse and the emergence of convective rolls. The convective rolls enhanced the mixing between solutions of A and B, leading to the increase in the volume of the nanodroplets. However, the scaling law between Pe and total volume is still valid because the convective rolls only affect the prefactors in Equation (5).

5.2.2. Effects on asphaltene precipitation

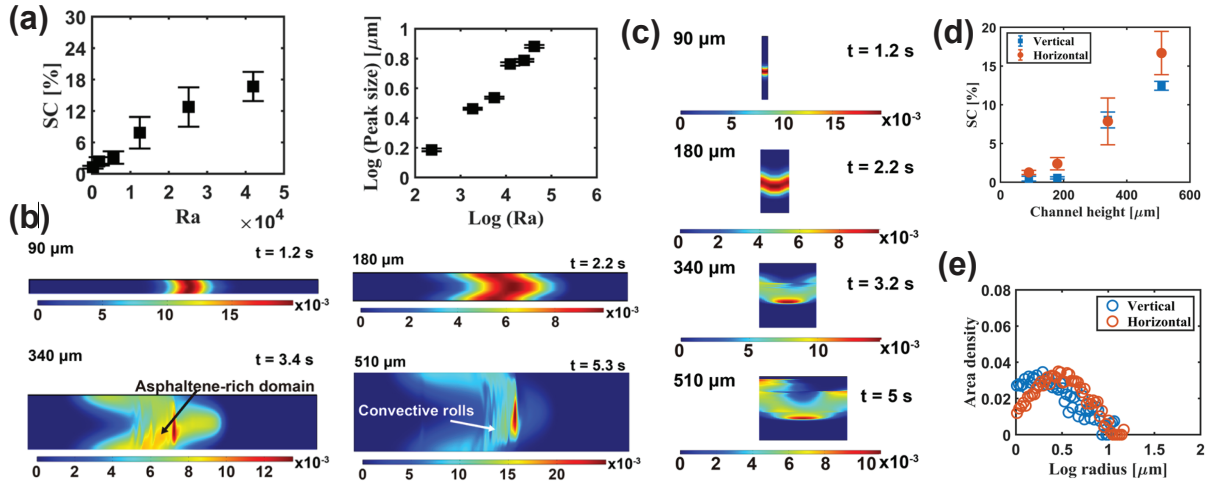


Figure 12: (a) Effect of channel heights on surface coverage and size of asphaltene particles. COMSOL simulation to show the flow profile in different channel heights of (b) horizontally and (c) vertically placed devices. Effect of orientation on (d) surface coverage and (e) size distribution of asphaltene particles [108]. Panels (a)-(e) are reproduced with permission from ref [108]. Copyright 2020 Elsevier.

COMSOL simulation visualized that the convective rolls also exist in the asphaltene system. The mixing is thus enhanced, and an asphaltene-rich domain appears at the tail of the mixing front, as shown in Figure

12(b). The mass transfer of asphaltene from the flow to the substrate is enhanced due to the longer transfer time and concentration gradient. Therefore, compared with the vertically placed device, the horizontal group shows a higher surface coverage and larger size, as shown in Figure 12(d)(e) [108].

6. Challenges and Future Perspectives

In analogy to the formation of nanodroplets induced by the Ouzo effect, a recent study has revealed the effect of mixing dynamics on the asphaltene precipitation. The previous studies on nanodroplet formation can be used as references for the study of asphaltene precipitation. However, the two processes are not the same because asphaltene is more complex and heterogeneity in molecular structures.

Researchers have demonstrated that mixing conditions affect asphaltene precipitation dynamics while solvent consumption remains constant. Nevertheless, a systematic correlation does not exist. Despite its importance, this aspect of the research has received insufficient attention. Understanding the fundamental insights helps to advance microscopy, microfluidics, and computational fluid dynamics. Asphaltene precipitation can be visualized at micro and nanometers. A microfluidic device can be designed to control mixing conditions, and simulation software can be used to characterize flow conditions. The following directions can be considered by researchers in the future.

1. Understand the effects of molecular structures of the asphaltene on the precipitation under different mixing conditions. Asphaltene of different molecule structures and molecular weight differ in their interactions with each other and the surrounding solvent. It is impossible to isolate and obtain asphaltenes of the same molecular structures. But it will be insightful and feasible to study precipitations of several fractions where the asphaltenes with similar sizes are grouped together. The more quantitative study will help to understand the intermolecular forces between asphaltene molecules to enhance the development of more reliable and predictive models.
2. computational fluid dynamics (CFD) tools can be utilized to correlate the mixing conditions with the yield and size distribution of asphaltene particles. The current study of the effects of mixing dynamics on asphaltene precipitation is still preliminary because of limited mixing regimes. The strong light-adsorbing nature of asphaltenes also limits the in-situ experimental study of the effects from the mixing dynamics. The flow and composition of liquids may be visualized in CFD simulations as the physical properties of the solutions are defined, including density, viscosity, and temperature. Correlating the CFD results with the experimental asphaltene yield and particle size distribution may help further understanding the effects of mixing on asphaltene precipitation.
3. Molecular spectroscopes with even higher spatial resolution can be used to characterize the finer morphology of asphaltene precipitates of known composition. The process of asphaltene precipitation from nano-aggregates to micron-sized particles in the current study is still challenging to be followed in

time. The particle size obtained by terminating the aggregation process at the early phase separation stage may be below the visible range of the conventional optical microscope. With the advancement of super-resolution microscopic technology, it may be possible to obtain high-resolution morphology and chemical composition simultaneously. The morphology may be therefore correlated with the molecular structures of asphaltenes and the aggregation process of asphaltene from nano-aggregates to microparticles.

4. Removal of the good solvent from the mixture to induce asphaltene precipitation. Preferential evaporation or dissolution of the good solvent from drops of a ternary mixture can also trigger the droplet formation [112–114], following the same mechanism for standard ouzo effect from the addition of the poor solvent, but in a reverse direction by reducing the ratio of the good solvent. Extremely rich transport phenomena driven Marangoni effect may occur during the evaporation or dissolution of the ouzo drops. Considering the drastically different interfacial tension and diffusion constants of the composition, it will be intriguing to study the effects of the selective solvent removal on asphaltene precipitation and explore how far the understanding based on well-defined aqueous systems can be applied to multicomponent organic mixtures of high complexity. Such a study may not be closely related to large-scale applications, but it contributes to a fundamental understand of phase separation in complex systems.

Table 4: Summary of conditions to form PSMPs.

Solution A	Solution B	Mixing conditions	Inhibitor
17 g/L asphaltene in toluene	70 % n-pentane	Diffusive- dominated	No
	80 % n-pentane		
	90 % n-pentane		
	100 % n-pentane		
	70 % n-heptane		
	80 % n-heptane		
	90 % n-heptane		
	100 % n-heptane		
	70 % n-decane		
	80 % n-decane		
	90 % n-decane		
	100 % n-decane		
	70 % n-pentane		Yes
	80 % n-pentane		
	90 % n-pentane		
	100 % n-pentane		
	70 % n-heptane		
	80 % n-heptane		
	90 % n-heptane		
	100 % n-heptane		
	100 % n-heptane	Solvent exchange	No
100 g/L bitumen in toluene	100 % n-heptane	Diffusive- dominated	No

7. Conclusions

Phase separation induced by the ouzo effect is a good analogy for understanding asphaltene precipitation. The droplet size from phase separation induced by the ouzo effect is determined by the chemical composition and mixing conditions. By leveraging advanced microfluidic techniques, the influence of mixing conditions on the ouzo effect can be well controlled. In parallel, asphaltene precipitation is a complex process influenced by thermodynamic factors, including the S/B ratio and type of precipitant. The use of microfluidic devices has brought about a turning point for understanding the effects of mixing dynamics [18]. Primary submicron particles form ubiquitously from mixing with the diluent under a wide range of mixing conditions. Without changing the use of solvent, the total yield of asphaltene and particle size can be adjusted by changing the mixing conditions. New techniques such as confocal and TIRF are complemented with computational fluid dynamics simulations to quantitatively understand the effects of mixing dynamics on asphaltene precipitation.

Many physico and hydrodynamical features are shared by the ouzo effect or nanoprecipitation in multicomponent aqueous systems and diluent-induced asphaltene precipitation. We hope that the comparison in this review will inspire more in-depth understanding of both asphaltene precipitation and the ouzo effect in aqueous systems.

Declaration of Competing Interests

The authors declare that they have no known competing financial interests or personal relationships that could have appeared to influence the work reported in this paper.

Biographies

Jia Meng received his Ph.D. degree in Chemical and Materials Engineering under the supervision of Prof. Xuehua Zhang from the University of Alberta, Edmonton, AB, Canada. His areas of research include soft matter and interface, microfluidic technology, and oil sands extraction.

Somasekhara Goud Sontti is a Postdoctoral researcher working in the Department of Chemical and Materials Engineering under the supervision of Prof. Xuehua Zhang at the University of Alberta, Canada. Dr. Sontti obtained his Ph.D. and M. Tech degrees in Chemical Engineering from the Indian Institute of Technology Kharagpur and the Indian Institute of Technology Guwahati, India. His research interest includes the broad area of multiphase flow, microfluidics, computational fluid dynamics, and slurry transport.

Xuehua Zhang is a Professor and Canada Research Chair (Tier 1) at the Department of Chemical and Materials Engineering, University of Alberta, Canada. Before, she worked at Australian National University, University of Melbourne, and RMIT University, Australia. The present research interests of Dr. Zhang range from microscopic bubbles and drops in separation technology and water treatment to evaporation and chemical reactions of droplets for ultrasensitive detection. She conducts both fundamental and applied research and combines experimental, theoretical, and numerical methods.

Acknowledgement

The authors are genuinely grateful for the inspiring discussions with Xiaoli Tan and Murray R Gary over the topic over the years. The authors acknowledge the support from Natural Science and Engineering Research Council of Canada (NSERC)–Collaborative Research and Development Grants, the Canada Research Chair Program, and from Canada Foundation for Innovation, John R. Evans Leaders Fund. This work is partially supported by the Canada Research Chairs program.

References

- [1] S. D. Taylor, J. Czarnecki, J. Masliyah, Refractive index measurements of diluted bitumen solutions, *Fuel* 80 (2001) 2013–2018.
- [2] F. Rao, Q. Liu, Froth treatment in athabasca oil sands bitumen recovery process: A review, *Energy Fuels* 27 (2013) 7199–7207.
- [3] Y. Xu, Asphaltene precipitation in paraffinic froth treatment: Effects of solvent and temperature, *Energy Fuels* 32 (2018) 2801–2810.
- [4] E. J. Hristova, S. R. Stoyanov, Bitumen froth treatment in the transition region between paraffinic and naphthenic process conditions, *Fuel* 286 (2021) 119385.
- [5] X. Zhang, Z. Lu, H. Tan, L. Bao, Y. He, C. Sun, D. Lohse, Formation of surface nanodroplets under controlled flow conditions, *Proc. Natl. Acad. Sci.* 112 (2015) 9253–9257.
- [6] S. A. Vitale, J. L. Katz, Liquid droplet dispersions formed by homogeneous liquid- liquid nucleation: The ouzo effect, *Langmuir* 19 (2003) 4105–4110.
- [7] T. N. Zemb, M. Klossek, T. Lopian, J. Marcus, S. Schöetl, D. Horinek, S. F. Prevost, D. Touraud, O. Diat, S. Marčelja, et al., How to explain microemulsions formed by solvent mixtures without conventional surfactants, *Proc. Natl. Acad. Sci.* 113 (2016) 4260–4265.
- [8] M. Rezaee, Y. Assadi, M.-R. M. Hosseini, E. Aghaee, F. Ahmadi, S. Berijani, Determination of organic compounds in water using dispersive liquid–liquid microextraction, *J. Chromatogr. A* 1116 (2006) 1–9.
- [9] X. H. Zhang, A. Quinn, W. A. Ducker, Nanobubbles at the interface between water and a hydrophobic solid, *Langmuir* 24 (2008) 4756–4764.
- [10] S. Schubert, J. T. Delaney Jr, U. S. Schubert, Nanoprecipitation and nanoformulation of polymers: from history to powerful possibilities beyond poly (lactic acid), *Soft Matter* 7 (2011) 1581–1588.
- [11] J. Aubry, F. Ganachaud, J.-P. Cohen Addad, B. Cabane, Nanoprecipitation of polymethylmethacrylate by solvent shifting: 1. boundaries, *Langmuir* 25 (2009) 1970–1979.
- [12] E. Lepeltier, C. Bourgaux, P. Couvreur, Nanoprecipitation and the ouzo effect: Application to drug delivery devices, *Adv. Drug Deliv. Rev.* 71 (2014) 86–97.
- [13] M. R. Gray, H. W. Yarranton, M. L. Chacon-Patino, R. P. Rodgers, B. Bouyssiere, P. Giusti, Distributed properties of asphaltene nanoaggregates in crude oils: A review, *Energy Fuels* 35 (2021) 18078–18103.
- [14] S. Mozaffari, H. Ghasemi, P. Tchoukov, J. Czarnecki, N. Nazemifard, Lab-on-a-chip systems in asphaltene characterization: a review of recent advances, *Energy Fuels* 35 (2021) 9080–9101.
- [15] I. Mohammed, M. Mahmoud, D. Al Shehri, A. El-Husseiny, O. Alade, Asphaltene precipitation and deposition: A critical review, *J. Pet. Sci. Eng.* 197 (2021) 107956.
- [16] F. Saghandali, M. Baghban Salehi, R. Hosseinzadehsemmnani, R. G. Moghanloo, V. Taghikhani, A review on chemical sand production control techniques in oil reservoirs, *Energy Fuels* 36 (2022) 5185–5208.
- [17] C. Yuan, W.-f. Pu, M. A. Ifticene, S. Zhao, M. A. Varfolomeev, Crude oil oxidation in an air injection based enhanced oil recovery process: Chemical reaction mechanism and catalysis, *Energy Fuels* 36 (2022) 5209–5227.
- [18] M. K. Sharma, R. L. Hartman, Perspectives on microfluidics for the study of asphaltenes in upstream hydrocarbon production: A minireview, *Energy Fuels* (2022).
- [19] Z. Lu, H. Xu, H. Zeng, X. Zhang, Solvent effects on the formation of surface nanodroplets by solvent exchange, *Langmuir* 31 (2015) 12120–12125.
- [20] C. Xu, H. Yu, S. Peng, Z. Lu, L. Lei, D. Lohse, X. Zhang, Collective interactions in the nucleation and growth of surface droplets, *Soft Matter* 13 (2017) 937–944.

- [21] D. Carteau, I. Pianet, P. Brunerie, B. Guillemat, D. M. Bassani, Probing the initial events in the spontaneous emulsification of trans-anethole using dynamic nmr spectroscopy, *Langmuir* 23 (2007) 3561–3565.
- [22] F. Ganachaud, J. L. Katz, Nanoparticles and nanocapsules created using the ouzo effect: spontaneous emulsification as an alternative to ultrasonic and high-shear devices, *ChemPhysChem* 6 (2005) 209–216.
- [23] E. Scholten, E. van der Linden, H. This, The life of an anise-flavored alcoholic beverage: Does its stability cloud or confirm theory?, *Langmuir* 24 (2008) 1701–1706.
- [24] J. Qian, G. F. Arends, X. Zhang, Surface nanodroplets: formation, dissolution, and applications, *Langmuir* 35 (2019) 12583–12596.
- [25] M. Li, H. Yu, L. Bao, B. Dyett, X. Zhang, Controlled addition of new liquid component into surface droplet arrays by solvent exchange, *J. Colloid Interface Sci.* 543 (2019) 164–173.
- [26] Y. Wang, B. Zeng, Y. Zhao, S. Li, X. Zhang, Formation of polystyrene microlenses via transient droplets from the ouzo effect for enhanced optical imaging, *J. Phys. Chem. C* 123 (2019) 14327–14337.
- [27] S. Prévost, S. Krickl, S. Marčelja, W. Kunz, T. Zemb, I. Grillo, Spontaneous ouzo emulsions coexist with pre-ouzo ultraflexible microemulsions, *Langmuir* 37 (2021) 3817–3827.
- [28] H. W. Yarranton, D. Ortiz, D. Barrera, E. Baydak, L. Barré, D. Frot, J. Eyssautier, H. Zeng, Z. Xu, G. Dechaine, et al., On the size distribution of self-associated asphaltenes, *Energy Fuels* 27 (2013) 5083–5106.
- [29] A. Soleymanzadeh, M. Yousefi, S. Kord, O. Mohammadzadeh, A review on methods of determining onset of asphaltene precipitation, *J. Pet. Explor. Prod. Technol.* 9 (2019) 1375–1396.
- [30] O. C. Mullins, H. Sabbah, J. Eyssautier, A. E. Pomerantz, L. Barré, A. B. Andrews, Y. Ruiz-Morales, F. Mostowfi, R. McFarlane, L. Goual, et al., Advances in asphaltene science and the yen–mullins model, *Energy Fuels* 26 (2012) 3986–4003.
- [31] M. Schulze, M. P. Lechner, J. M. Stryker, R. R. Tykwinski, Aggregation of asphaltene model compounds using a porphyrin tethered to a carboxylic acid, *Org. Biomol. Chem.* 13 (2015) 6984–6991.
- [32] M. R. Gray, R. R. Tykwinski, J. M. Stryker, X. Tan, Supramolecular assembly model for aggregation of petroleum asphaltenes, *Energy Fuels* 25 (2011) 3125–3134.
- [33] A. Zahabi, M. R. Gray, J. Czarnecki, T. Dabros, Flocculation of silica particles from a model oil solution: effect of adsorbed asphaltenes, *Energy Fuels* 24 (2010) 3616–3623.
- [34] S. Wang, J. Liu, L. Zhang, Z. Xu, J. Masliyah, Colloidal interactions between asphaltene surfaces in toluene, *Energy Fuels* 23 (2009) 862–869.
- [35] S. Wang, J. Liu, L. Zhang, J. Masliyah, Z. Xu, Interaction forces between asphaltene surfaces in organic solvents, *Langmuir* 26 (2010) 183–190.
- [36] A. F. Barton, *CRC handbook of solubility parameters and other cohesion parameters*, Routledge, 2017.
- [37] S. Fakher, A. Imqam, Asphaltene precipitation and deposition during co₂ injection in nano shale pore structure and its impact on oil recovery, *Fuel* 237 (2019) 1029–1039.
- [38] N. H. Rahmani, J. H. Masliyah, T. Dabros, Characterization of asphaltenes aggregation and fragmentation in a shear field, *AIChE J.* 49 (2003) 1645–1655.
- [39] Y. Zhuang, A. Goharzadeh, Y. J. Lin, Y. F. Yap, J. Chai, N. Mathew, F. Vargas, S. L. Biswal, Three dimensional measurements of asphaltene deposition in a transparent micro-channel, *J. Pet. Sci. Eng.* 145 (2016) 77–82.
- [40] M. Tavakkoli, M. R. Grimes, X. Liu, C. K. Garcia, S. C. Correa, Q. J. Cox, F. M. Vargas, Indirect method: a novel technique for experimental determination of asphaltene precipitation, *Energy Fuels* 29 (2015) 2890–2900.
- [41] X. Li, Y. Guo, Q. Sun, W. Lan, A. Liu, X. Guo, Experimental study for the impacts of flow rate and concentration of asphaltene precipitant on dynamic asphaltene deposition in microcapillary medium, *J. Pet. Sci. Eng.* 162 (2018) 333–340.
- [42] H. Alboudwarej, K. Akbarzadeh, J. Beck, W. Y. Svrcek, H. W. Yarranton, Regular solution model for asphaltene

- precipitation from bitumens and solvents, *AIChE J.* 49 (2003) 2948–2956.
- [43] L. B. d. S. Balestrin, R. D. Francisco, C. A. Bertran, M. B. Cardoso, W. Loh, Direct assessment of inhibitor and solvent effects on the deposition mechanism of asphaltenes in a brazilian crude oil, *Energy Fuels* 33 (2019) 4748–4757.
 - [44] I. Yudin, G. Nikolaenko, E. Gorodetskii, V. Kosov, V. Melikyan, E. Markhashov, D. Frot, Y. Briolant, Mechanisms of asphaltene aggregation in toluene–heptane mixtures, *J. Pet. Sci. Eng.* 20 (1998) 297–301.
 - [45] X. Li, Y. Guo, E. S. Boek, X. Guo, Experimental study on kinetics of asphaltene aggregation in a microcapillary, *Energy Fuels* 31 (2017) 9006–9015.
 - [46] C. M. Seifried, J. Crawshaw, E. S. Boek, Kinetics of asphaltene aggregation in crude oil studied by confocal laser-scanning microscopy, *Energy Fuels* 27 (2013) 1865–1872.
 - [47] B. K. Johnson, R. K. Prud homme, Mechanism for rapid self-assembly of block copolymer nanoparticles, *Phys. Rev. Lett.* 91 (2003) 118302.
 - [48] C. Zhao, S. Melis, E. P. Hughes, T. Li, X. Zhang, P. D. Olmsted, E. Van Keuren, Particle formation mechanisms in the nanoprecipitation of polystyrene, *Langmuir* 36 (2020) 13210–13217.
 - [49] M. Beck-Broichsitter, Solvent impact on polymer nanoparticles prepared nanoprecipitation, *Colloids Surf. A: Physicochem. Eng. Asp.* 625 (2021) 126928.
 - [50] Z. Li, H. Zeng, X. Zhang, Growth rates of hydrogen microbubbles in reacting femtoliter droplets, *Langmuir* 38 (2022) 6638–6646.
 - [51] J. Meng, J. B. You, X. Zhang, Viscosity-mediated growth and coalescence of surface nanodroplets, *J. Phys. Chem. C* . 124 (2020) 12476–12484.
 - [52] H. Yu, Z. Lu, D. Lohse, X. Zhang, Gravitational effect on the formation of surface nanodroplets, *Langmuir* 31 (2015) 12628–12634.
 - [53] H. W. Yarranton, F. Ramos-Pallares, Regular solution theory applied to asphaltene related phase behaviour, *Can. J. Chem. Eng.* 99 (2021) 1050–1067.
 - [54] S. Enayat, N. R. Babu, J. Kuang, S. Rezaee, H. Lu, M. Tavakkoli, J. Wang, F. M. Vargas, On the development of experimental methods to determine the rates of asphaltene precipitation, aggregation, and deposition, *Fuel* 260 (2020) 116250.
 - [55] J. Kuang, M. Tavakkoli, J. Yarbrough, J. Wang, S. Jain, S. Ashtekar, D. S. Abdallah, S. Punnapala, F. M. Vargas, Investigation of asphaltene deposition at high temperature and under dynamic conditions, *Energy Fuels* 32 (2018) 12405–12415.
 - [56] X. Li, Y. Guo, E. S. Boek, X. Guo, Experimental study on kinetics of asphaltene aggregation in a microcapillary, *Energy Fuels* 31 (2017) 9006–9015.
 - [57] M. Mohammadi, M. Akbari, Z. Fakhroueian, A. Bahramian, R. Azin, S. Arya, Inhibition of asphaltene precipitation by tio₂, sio₂, and zro₂ nanofluids, *Energy Fuels* 25 (2011) 3150–3156.
 - [58] Y. Long, T. Dabros, H. Hamza, Structure of water/solids/asphaltenes aggregates and effect of mixing temperature on settling rate in solvent-diluted bitumen, *Fuel* 83 (2004) 823–832.
 - [59] N. Haji-Akbari, P. Masirisuk, M. P. Hoepfner, H. S. Fogler, A unified model for aggregation of asphaltenes, *Energy Fuels* 27 (2013) 2497–2505.
 - [60] Y.-F. Hu, T.-M. Guo, Effect of temperature and molecular weight of n-alkane precipitants on asphaltene precipitation, *Fluid Ph. Equilibria* 192 (2001) 13–25.
 - [61] I. A. Wiehe, H. W. Yarranton, K. Akbarzadeh, P. M. Rahimi, A. Teclemariam, The paradox of asphaltene precipitation with normal paraffins, *Energy Fuels* 19 (2005) 1261–1267.
 - [62] J. Zawala, T. Dabros, H. A. Hamza, Settling properties of aggregates in paraffinic froth treatment, *Energy Fuels* 26 (2012) 5775–5781.

- [63] N. H. Rahmani, T. Dabros, J. H. Masliyah, Fractal structure of asphaltene aggregates, *J. Colloid Interface Sci.* 285 (2005) 599–608.
- [64] N. H. Rahmani, T. Dabros, J. H. Masliyah, Evolution of asphaltene floc size distribution in organic solvents under shear, *Chem. Eng. Sci.* 59 (2004) 685–697.
- [65] M. Torkaman, M. Bahrami, M. R. Dehghani, Influence of temperature on aggregation and stability of asphaltenes. ii. orthokinetic aggregation, *Energy Fuels* 32 (2018) 6144–6154.
- [66] D. D. Nguyen, R. Daneshfar, A. H. S. Dehaghani, C.-H. Su, The effect of shear rate on aggregation and breakage of asphaltenes flocs: Experimental study and model-based analysis, *J. Mol. Liq.* 325 (2021) 114861.
- [67] J. Pandya, L. Spielman, Floc breakage in agitated suspensions: effect of agitation rate, *Chem. Eng. Sci.* 38 (1983) 1983–1992.
- [68] A. R. Solaimany-Nazar, H. Rahimi, Dynamic determination of asphaltene aggregate size distribution in shear induced organic solvents, *Energy Fuels* 22 (2008) 3435–3442.
- [69] M. Igder, N. Hosseinpour, A. A. Biyouki, A. Bahramian, Control of asphaltene aggregation in reservoir model oils along the production streamline by Fe_3O_4 and NiO nanoparticles, *Energy Fuels* 32 (2018) 6689–6697.
- [70] H. Chen, A. E. Celik, A. Mutschler, A. Combes, A. Runser, A. S. Klymchenko, S. Lecommandoux, C. A. Serra, A. Reisch, Assembly of fluorescent polymer nanoparticles using different microfluidic mixers, *Langmuir* 38 (2022) 7945–7955.
- [71] M. Abdelkarim, N. H. Abd Ellah, M. Elsabahy, M. Abdelgawad, S. A. Abouelmagd, Microchannel geometry vs flow parameters for controlling nanoprecipitation of polymeric nanoparticles, *Colloids Surf. A: Physicochem. Eng. Asp.* 611 (2021) 125774.
- [72] E. S. Boek, H. K. Ladva, J. P. Crawshaw, J. T. Padding, Deposition of colloidal asphaltene in capillary flow: experiments and mesoscopic simulation, *Energy Fuels* 22 (2008) 805–813.
- [73] K. A. Lawal, J. P. Crawshaw, E. S. Boek, V. Vesovic, Experimental investigation of asphaltene deposition in capillary flow, *Energy Fuels* 26 (2012) 2145–2153.
- [74] E. S. Boek, A. D. Wilson, J. T. Padding, T. F. Headen, J. P. Crawshaw, Multi-scale simulation and experimental studies of asphaltene aggregation and deposition in capillary flow, *Energy Fuels* 24 (2010) 2361–2368.
- [75] Y. Zhuang, A. Goharzadeh, Y. J. Lin, Y. F. Yap, J. Chai, N. Mathew, F. Vargas, S. L. Biswal, Experimental study of asphaltene deposition in transparent microchannels using the light absorption method, *J. Dispers. Sci. Technol.* 39 (2018) 744–753.
- [76] Y.-J. Lin, T. Cao, M. L. Chacón-Patiño, S. M. Rowland, R. P. Rodgers, A. Yen, S. L. Biswal, Microfluidic study of the deposition dynamics of asphaltene subfractions enriched with island and archipelago motifs, *Energy Fuels* 33 (2019) 1882–1891.
- [77] C. Hu, J. E. Morris, R. L. Hartman, Microfluidic investigation of the deposition of asphaltenes in porous media, *Lab Chip* 14 (2014) 2014–2022.
- [78] Y.-J. Lin, P. He, M. Tavakkoli, N. T. Mathew, Y. Y. Fatt, J. C. Chai, A. Goharzadeh, F. M. Vargas, S. L. Biswal, Examining asphaltene solubility on deposition in model porous media, *Langmuir* 32 (2016) 8729–8734.
- [79] Y.-J. Lin, P. He, M. Tavakkoli, N. T. Mathew, Y. Y. Fatt, J. C. Chai, A. Goharzadeh, F. M. Vargas, S. L. Biswal, Characterizing asphaltene deposition in the presence of chemical dispersants in porous media micromodels, *Energy Fuels* 31 (2017) 11660–11668.
- [80] A. S. Shalygin, I. V. Kozhevnikov, S. G. Kazarian, O. N. Martyanov, Spectroscopic imaging of deposition of asphaltenes from crude oil under flow, *J. Pet. Sci. Eng.* 181 (2019) 106205.
- [81] Z. Qi, A. Abedini, A. Sharbatian, Y. Pang, A. Guerrero, D. Sinton, Asphaltene deposition during bitumen extraction with natural gas condensate and naphtha, *Energy Fuels* 32 (2018) 1433–1439.
- [82] K. Keshmiri, H. Huang, N. Nazemifard, Microfluidic platform to evaluate asphaltene deposition during solvent-based

- extraction of bitumen, *Fuel* 239 (2019) 841–851.
- [83] Q. Lin, T. Akai, M. J. Blunt, B. Bijeljic, H. Iwama, K. Takabayashi, Y. Onaka, H. Yonebayashi, Pore-scale imaging of asphaltene-induced pore clogging in carbonate rocks, *Fuel* 283 (2021) 118871.
 - [84] R. Mokhtari, A. Hosseini, M. Fatemi, S. I. Andersen, S. Ayatollahi, Asphaltene destabilization in the presence of an aqueous phase: The effects of salinity, ion type, and contact time, *J. Pet. Sci. Eng.* 208 (2022) 109757.
 - [85] Z. Lu, M. H. K. Schaarsberg, X. Zhu, L. Y. Yeo, D. Lohse, X. Zhang, Universal nanodroplet branches from confining the ouzo effect, *Proc. Natl. Acad. Sci.* 114 (2017) 10332–10337.
 - [86] J. Meng, S. G. Sontti, M. Sadeghi, G. F. Arends, P. Nikrityuk, X. Tan, X. Zhang, Size distribution of primary submicron particles and larger aggregates in solvent-induced asphaltene precipitation in a model oil system, *Fuel* 322 (2022) 124057.
 - [87] J. Meng, J. B. You, G. F. Arends, H. Hao, X. Tan, X. Zhang, Microfluidic device coupled with total internal reflection microscopy for in situ observation of precipitation, *Eur. Phys. J. E* 44 (2021) 1–8.
 - [88] G. F. Arends, J. B. You, J. M. Shaw, X. Zhang, Enhanced displacement of phase separating liquid mixtures in 2d confined spaces, *Energy Fuels* 35 (2021) 5194–5205.
 - [89] G. F. Arends, J. M. Shaw, X. Zhang, How fast do microdroplets generated during liquid–liquid phase separation move in a confined 2d space?, *Energy Fuels* 35 (2021) 11257–11270.
 - [90] S. H. Lim, K. S. Go, N. S. Nho, J. G. Lee, Effect of reaction temperature and time on the products and asphaltene dispersion stability in slurry-phase hydrocracking of vacuum residue, *Fuel* 234 (2018) 305–311.
 - [91] J. Duran, Y. Casas, L. Xiang, L. Zhang, H. Zeng, H. Yarranton, Nature of asphaltene aggregates, *Energy Fuels* 33 (2018) 3694–3710.
 - [92] I. Struchkov, M. Rogachev, E. Kalinin, P. Roschin, Laboratory investigation of asphaltene-induced formation damage, *J. Pet. Explor. Prod. Technol.* 9 (2019) 1443–1455.
 - [93] J. Castillo, J. Hung, S. Goncalves, A. Reyes, Study of asphaltenes aggregation process in crude oils using confocal microscopy, *Energy Fuels* 18 (2004) 698–703.
 - [94] J. Hung, J. Castillo, A. Reyes, Kinetics of asphaltene aggregation in toluene–heptane mixtures studied by confocal microscopy, *Energy Fuels* 19 (2005) 898–904.
 - [95] M. Guo, P. Chandris, J. P. Giannini, A. J. Trexler, R. Fischer, J. Chen, H. D. Vishwasrao, I. Rey-Suarez, Y. Wu, X. Wu, et al., Single-shot super-resolution total internal reflection fluorescence microscopy, *Nat. Methods* 15 (2018) 425–428.
 - [96] C. Niederauer, P. Blumhardt, J. Mücksch, M. Heymann, A. Lambacher, P. Schwille, Direct characterization of the evanescent field in objective-type total internal reflection fluorescence microscopy, *Opt. Express* 26 (2018) 20492–20506.
 - [97] B. Dyett, A. Kiyama, M. Rump, Y. Tagawa, D. Lohse, X. Zhang, Growth dynamics of surface nanodroplets during solvent exchange at varying flow rates, *Soft matter* 14 (2018) 5197–5204.
 - [98] J. J. Axelrod, D. Axelrod, Light scattering in tirf microscopy: A theoretical study of the limits to surface selectivity, *Biophys. J.* 120 (2021) 2952–2968.
 - [99] J. Meng, J. B. You, H. Hao, X. Tan, X. Zhang, Primary submicron particles from early stage asphaltene precipitation revealed in situ by total internal reflection fluorescence microscopy in a model oil system, *Fuel* 296 (2021) 120584.
 - [100] B. Zeng, Y. Wang, X. Zhang, D. Lohse, Solvent exchange in a hele–shaw cell: Universality of surface nanodroplet nucleation, *J. Phys. Chem. C* . 123 (2019) 5571–5577.
 - [101] B. Dyett, H. Yu, X. Zhang, Formation of surface nanodroplets of viscous liquids by solvent exchange, *Eur. Phys. J. E* 40 (2017) 1–6.
 - [102] M. Li, L. Bao, H. Yu, X. Zhang, Formation of multicomponent surface nanodroplets by solvent exchange, *J. Phys. Chem. C* . 122 (2018) 8647–8654.
 - [103] D. Lohse, X. Zhang, et al., Surface nanobubbles and nanodroplets, *Rev. Mod. Phys.* 87 (2015) 981.
 - [104] H. Wang, Z. Wei, S. I. Vagin, X. Zhang, B. Rieger, A. Meldrum, Ultrasensitive picomolar detection of aqueous acids in

- microscale fluorescent droplets, *ACS Sens.* 7 (2021) 245–252.
- [105] X. H. Zhang, W. Ducker, Formation of interfacial nanodroplets through changes in solvent quality, *Langmuir* 23 (2007) 12478–12480.
 - [106] J. B. You, D. Lohse, X. Zhang, Tuning composition of multicomponent surface nanodroplets in a continuous flow-in system, *Adv. Mater. Interfaces* 8 (2021) 2101126.
 - [107] D. Lohse, X. Zhang, Physicochemical hydrodynamics of droplets out of equilibrium, *Nat. Rev. Phys.* 2 (2020) 426–443.
 - [108] J. Meng, C. Kanike, S. G. Sontti, A. Atta, X. Tan, X. Zhang, Asphaltene precipitation under controlled mixing conditions in a microchamber, *Chem. Eng. J.* 451 (2023) 138873.
 - [109] S. H. Abbas Rizvi, A. Yadav, J. Phirani, V. Singh, Deposition and removal studies of asphaltene from the glass surface, *Energy Fuels* 35 (2021) 3228–3239.
 - [110] O. Elkhatab, W. Chaisoontornyotin, M. Geshe, L. Goual, Nanoscale investigation of asphaltene deposition under capillary flow conditions, *Energy Fuels* 34 (2019) 5148–5158.
 - [111] H. Sarsito, S. Alkafeef, J. C. Berg, Suppression of asphaltene adsorption and deposition in porous media, *Energy Fuels* 35 (2021) 16553–16561.
 - [112] H. Tan, C. Diddens, P. Lv, J. G. M. Kuerten, X. Zhang, D. Lohse, Evaporation-triggered microdroplet nucleation and the four life phases of an evaporating ouzo drop, *Proceedings of the National Academy of Sciences* 113 (2016) 8642–8647.
 - [113] H. Tan, C. Diddens, M. Versluis, H.-J. Butt, D. Lohse, X. Zhang, Self-wrapping of an ouzo drop induced by evaporation on a superamphiphobic surface, *Soft Matter* 13 (2017) 2749–2759.
 - [114] H. Tan, C. Diddens, A. A. Mohammed, J. Li, M. Versluis, X. Zhang, D. Lohse, Microdroplet nucleation by dissolution of a multicomponent drop in a host liquid, *J. Fluid Mech.* 870 (2019) 217–246.